Surprisingly short-ranged interactions in highly charged colloidal suspensions

Richard V. Durand and Carl Franck
Laboratory of Atomic and Solid State Physics and Center for Materials Research, Cornell University, Ithaca, New York 14853-2501
(Received 20 January 2000)

The interaction potential between colloidal particles in a suspension has been the topic of much research recently. Digital video microscopy techniques have come into wide use, as this method yields direct information about the structure of such systems. However, two main problems have plagued researchers working with this technique. First, what one sees through a microscope is actually a projection of a three-dimensional sample onto a two-dimensional image plane. Second, in order to achieve long-range interactions between particles, the ionicity of the surrounding medium must be as low as possible. In order to address the first problem, researchers have created quasi-two-dimensional samples by confining the system between two glass plates. However, this geometry makes it difficult to control the ionicity, and it also makes the analysis more difficult since one is dealing with an anisotropic system for which established theories of colloidal interactions formulated for the bulk do not apply. We have developed techniques to effectively address each of these two problems. Our sample cell is large enough to allow direct contact of the suspension with ion exchange resin, and allows one to make bulk measurements of the structure. In addition, we have developed techniques to handle the projection effects. We have used these methods to measure the radial distribution function of dilute suspensions of highly charged unconfined polystyrene microspheres in a density matched mixture of H_2O and D_2O. We found that the interaction potential between the colloidal particles was much shorter ranged than would be expected based on the Derjaguin-Landau-Verwey-Overbeek theory of colloidal interactions.

PACS number(s): 82.70.Dd, 61.20.−p

I. INTRODUCTION

Colloidal systems consisting of suspensions of charged spherical particles in aqueous media have been of especially strong recent interest [1–12]. If we ignore the surrounding suspending medium, the colloidal particles can be considered as ''atoms'' complete with a long-range interaction which can lead to both liquid and solid phases. As such, these systems are appealing because they provide a fertile testing ground for theories of both the liquid and solid states. An important component of any theoretical description of a colloidal system is the interparticle potential. This can be deduced by measuring the equilibrium structure of the system either through scattering or direct visualization techniques, i.e., microscopy. The former method yields the static structure factor $S(q)$, while the latter technique gives the radial distribution function (RDF) $g(r)$. There are several advantages to direct visualization techniques. Finding the RDF from microscopy data is experimentally easier, and requires much less data reduction effort than finding $S(q)$ from scattering data. Furthermore, direct visualization methods can reveal information about higher order correlations such as triplet distributions that cannot be obtained through scattering experiments. In addition, extracting the pairwise interaction from $S(q)$ is difficult because crucial information is contained in the low q region, which is difficult to access experimentally. In contrast, it is a trivial matter to extract the pairwise potential from the RDF in the limit of low number density using the Boltzmann relation $U(r) = -kT \ln g(r)$.

Direct visualization techniques have their deficiencies, however, as there are two main problems associated with the techniques. First, what one sees through a microscope is actually a projection of a three-dimensional sample onto a two-dimensional image plane, and therefore, information is lost concerning the particle position in the direction perpendicular to the image plane. Second, in order to achieve long-range interactions between particles, the ionicity of the surrounding medium must be as low as possible. In order to address the first problem, researchers have created quasi-two-dimensional samples by confining the system between two glass plates [3,5,6]. However, this geometry makes it difficult to control the ionicity, and it also makes the analysis more difficult since one is dealing with an anisotropic system for which established theories of colloidal interactions formulated for the bulk do not apply.

We have developed techniques to effectively address each of these two problems. Our sample cell is large enough to allow direct contact of the suspension with ion exchange resin, and allows one to make bulk measurements of the structure. In addition, we have developed techniques to handle the projection effects, which include systematically reducing the effective depth of field by digital image processing methods, and an algorithm that extracts a three-dimensional RDF from two-dimensional microscopy data. We have used these methods to measure the RDF of dilute suspensions of highly charged unconfined polystyrene microspheres (of diameter 0.979 μm) in a density matched mixture of H_2O and D_2O. We found that the interaction potential between the colloidal particles was much shorter ranged than would be expected based on our understanding of the chemical environment of our samples and the Derjaguin-Landau-Verwey-Overbeek (DLVO) theory of colloidal interactions [13]. As will be shown in this paper, the Debye length in our samples was 0.11–0.20 μm, much shorter than the value of ≈ 1 μm which would be obtained in the purest possible aqueous environment, which we expected to be close to due to our careful sample preparation and close proximity of the particles to the ion exchange resin. Even

admitting the possibility of ionic contamination, we will argue that the Debye length should have been greater than 0.27 μm.

The organization of this paper is as follows. In Sec. II, we describe the sample preparation, data collection protocol, and data reduction techniques. We also present a technique for constructing a three-dimensional RDF from a two-dimensional microscope image. In Sec. III, we calculate the RDF's of our samples, and explain why the results are inconsistent with our understanding. In Sec. IV, we discuss some possible reasons for our unexpected results, and compare our results to those of other workers in this field. In Sec. V, we summarize our findings and give suggestions for future work.

II. EXPERIMENT

A. Sample preparation

The colloidal systems studied in this work consisted of suspensions of fluorescent polystyrene particles of diameter 0.979 ± 0.026 μm (Polysciences No. 15702). The particles had both sulfate and carboxylate surface groups, with parking areas of 6–8 and 0.1–0.8 nm^2, respectively [14], yielding approximately 4×10^5 sulfate groups and $(4–30) \times 10^6$ carboxylate groups per particle.

The suspending medium was a mixture of H_2O and D_2O ($51 \pm 1\%$ H_2O by volume) of density 1.05 g/cm^3, which is approximately the density of the polystyrene particles [14]. The sulfate and carboxylate surface groups dissociate when the particles are in solution, leading to a negative particle charge. The number density of particles ρ was studied over the range 10^{-4}–10^{-2} μm^{-3}. The sample cell consisted of a $7.5 \times 2.5 \times 0.12$-cm^3 glass microscope slide (soda lime, VWR Scientific No. 48300-036) with an oval shaped hole drilled into it. Two No. 1 1/2 cover slips (borosilicate, VWR Scientific No. 48366-227) were glued to each side of the hole using waterproof cement (Plumber's Goop, Eclectic Products, Inc.), forming a cavity of approximate dimensions $1.5 \times 1 \times 0.12$ cm^3. All glass parts were carefully cleaned prior to assembly [15]. A small hole was drilled into one of the cover slips in order to fill the cell. After the suspension was introduced into the cavity via a pipetter, a small square of glass cut from a No. 2 cover slip (zinc titanium, Corning No. 2875-18) was fitted over the hole, and waterproof cement was placed over the area. This formed a very tight seal with minimal contamination of the cell by the adhesive [16].

In addition to any residual ionic impurities in the water used for the suspension, the glass as well as the adhesive (in principle) can act as virtual leaks of ions (especially the drilled glass [17]). To remove these impurity ions, we inserted mixed bed ion exchange resin (Bio-Rad AG 501-X8) into the cells prior to filling. The resin occupied approximately 25% of the sample volumes, and was directly in contact with the suspension. The ion exchange resin replaces positive and negative ions in solution with H^+ and OH^- ions, respectively, which combine to form water. Thus, we assert that the presence of the D_2O did not interfere with the deionizing process. The ion exchange resin could move freely through the sample volume, and thus, by rotating the samples about an axis parallel to the 2.5-cm side (axis oriented horizontally), the resin was moved continuously through the suspension, which accelerated the deionization process. The samples were constructed 1–2 weeks prior to data collection, and were rotated at 0.2 Hz for a total of 20 h over the course of the two days prior to taking data.

Palberg *et al.* [7] developed a system in which a suspension can be continuously deionized by pumping it through a closed loop which contains ion exchange resin. They were able to completely deionize their specimens in approximately 1 h. We believe our rotation method and high volume fraction of resin should deionize on a similar time scale, and since we rotated our samples for 20 h, we assert that our samples were strongly deionized by this procedure. Later in this paper, we will present additional arguments in support of our decision to put ion exchange resin directly into the sample cell.

B. Data collection

Laser scanning confocal microscopy is the method of choice in studying colloidal suspensions, as it offers both high signal to noise ratio and small depth of field [18]. The images obtained are in digital format, which can subsequently be processed to yield the positions of the particles. The confocal microscope we used [19] was fitted with a piezo driver that allowed a very precise vertical sectioning of the sample up to 90 μm into the bulk. The suspension was viewed through the bottom cover slip using a water immersion objective of magnification 63$\times$ and working distance 220 μm, which, in the digitized images, yielded pixels of size 0.207×0.207 μm^2.

The analysis of the data is greatly simplified when the samples are isotropic. To achieve this, we rotated each sample as described in Sec. II A for approximately 30 min before taking data. The ion exchange resin thus played a dual role as stirrers and ion pumps. Each sample was placed on the microscope stage several minutes prior to taking data in order to allow the suspension to equilibrate, which is enough time for the particles to diffuse several characteristic interparticle distances $\rho^{-1/3}$.

For each sample, the position of the bottom cover slip was determined using the ''reflected light'' mode of the microscope. In this mode of operation, a bright flash is observed when the focal plane coincides with the glass-water interface at the bottom cover slip. This position was defined to be the zero position in the vertical, or z direction.

We examined five different suspensions with number densities varying from 2.3×10^{-4} to 8.0×10^{-3} μm^{-3}. These number densities were calculated using the manufacturer supplied value for the volume fraction 2.70% and the known dilutions used in preparing the samples. The data collected from each of the sample cells consisted of a series of microscopy images taken with the objective placed at uniformly spaced intervals $\Delta z = 1$ μm from $z = 10$ μm to $z = 90$ μm. Each image was formed over a time of 1/30 s, and the piezo driver required 1/30 s to move from one z level to the next. For each data set, 25–50 such z scans were performed. We started at $z = 10$ μm to ensure that the presence of the wall did not influence the colloidal structure in the region of interest, and we stopped at $z = 90$ μm because that was the maximum distance to which the piezo driver would reliably move. To correct for refractive effects, the distance moved

by the objective was multiplied by the refractive index of the suspending medium (1.33) to obtain the corresponding distance moved by the focal plane in the sample. Because the medium was density matched to the particles, sedimentation was minimized, and the sample stayed approximately isotropic over the data collection period, as verified by examining the number of particles versus z position.

C. Image analysis

In order to extract the RDF from the images, one must first identify which features in the images are particles, and then compute their positions. With confined suspensions, this task is made easier by the fact that only one layer of particles is seen, and the distance between particles is large compared to the size of a particle. In the present work, where we looked at a bulk specimen, a combination of projection effects and a surprisingly short-ranged interaction allowed particles to ''overlap'' in the images, which made our task more difficult.

To overcome these difficulties, we used a modified version of Crocker and Grier's algorithm [1] to extract the particles' positions from the images. We needed to adapt their method to allow greater flexibility in choosing various input parameters, due to the fact that our particles were not as well separated as those in Crocker and Grier's samples. Specifically, whereas in the Crocker-Grier (CG) algorithm, the length scales for the background subtraction [20], candidate particle selection [21], and moment calculation [22] were all the same, with our modifications we allowed different values for each. The intensity profile of a particle is approximately 5–6 pixels in diameter, somewhat larger than the physical diameter of 4.7 pixels. We chose a CG background subtraction length scale somewhat larger than the particle diameter, or 6–10 pixels. The CG candidate particle selection length scale was chosen to be approximately the diameter of the particle, or 4–5 pixels, while the CG moment calculation length scale was chosen to be approximately the radius of the particle, or 3–4 pixels.

Another modification to the algorithm included the option of finding the particle position by fitting the intensity profile $I(x,y)$ of the particle to a Gaussian of the form

$$I(x,y)=I_0\exp\left[-\frac{1}{2}\left(\frac{x-x_0}{\sigma_x}\right)^2-\frac{1}{2}\left(\frac{y-y_0}{\sigma_y}\right)^2\right], \qquad (1)$$

instead of using the intensity weighted centroid as in the Crocker-Grier method. When using a Gaussian fit to find the center of the intensity profile of a particle, one may use a smaller region of the particle than with the intensity weighted centroid method. In the latter method, one must integrate over the entire intensity profile, and, if another particle happens to be within the integration region, then the calculated centroid will be biased toward the nearby particle. Using a Gaussian fit, very good results are obtained by restricting the fit to a region well within the boundaries of the particle, thus reducing the biasing effect. Accordingly, the Gaussian fit was performed over a circular region of radius somewhat smaller than the particle radius, or 2–3 pixels.

There was some variation in how the images were analyzed. In some cases, no background subtraction was done, and in other cases, a smoothing operation was performed on the images prior to analysis. Sometimes a Gaussian fit was not performed, and the intensity weighted centroid was used to find the particles' positions. These variations did not significantly affect our results.

For each particle identified, the algorithm also gives a series of descriptive parameters about the particle such as the brightness [23], the radius of gyration [24], and the peak intensity [I_0 in Eq. (1)] as determined by the Gaussian fit (in cases where the Gaussian fit was used). Using these parameters, one can make cuts on the data to eliminate spuriously identified particles caused by fluctuations in the background intensity. These parameters can also be used to change the effective depth of field since particles become dimmer and less focused the further they are from the focal plane. This ability to change the effective depth of field is particularly important for our observations, where we are not looking at a monolayer of particles, but at a finite slice of a three dimensional system.

Once a series of coordinates representing the particles' positions have been found, it is straightforward to compute the RDF $g(r)$ using

$$g(r)=\frac{N(r)}{n2\pi r\Delta r}, \qquad (2)$$

where $N(r)$ is the number of particles in the neighborhood of a reference particle which are in a circular ring of inner and outer radii $r-\Delta r/2$ and $r+\Delta r/2$, respectively (averaged over all possible reference particles and images), and n is the two-dimensional number density of particles averaged over all images. To avoid boundary effects, we only use reference particles that are at least a distance r_{max} from the borders of the images, where r_{max} is the largest distance we want to consider, which in this work is 10 μm. In choosing the appropriate bin width Δr, one has to compromise between two competing factors. If Δr is too small, then there are few particles per bin and the statistics are poor. On the other hand, if Δr is too large, then significant smoothing of $g(r)$ occurs, and the discrete approximation given by Eq. (2) will depart significantly from the underlying continuous $g(r)$. We chose the smallest bin width that gave reasonably sized statistical errors, $\Delta r=0.2$–0.5 μm.

Note that this RDF is actually a two-dimensional, or projected, RDF because it was derived from data from a microscope image, which only contains two-dimensional coordinates. The present experiment was originally designed to take advantage of the z-scanning feature of the confocal microscope to obtain fully three-dimensional information about the particle positions. However, in order for this to be possible, the particles needed to be far enough apart so that the Brownian movement in the 1/30-s time period between z levels was negligible compared to the typical pair separation. As we will discuss later in this paper, the interaction range was much shorter than expected, so the above criterion was not satisfied, and we had to resort to a two-dimensional analysis of the data.

D. Dealing with projection effects

When the RDF is extracted from microscopy data, what is really being calculated is a ''projected'' RDF, since one is in

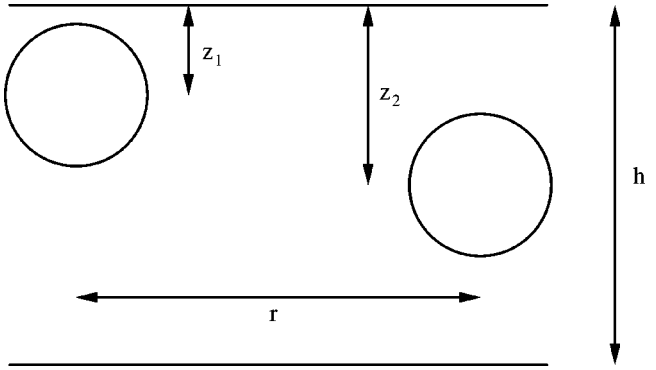

FIG. 1. A schematic picture of two colloidal particles in an observation volume of height h. Other position variables are defined in text.

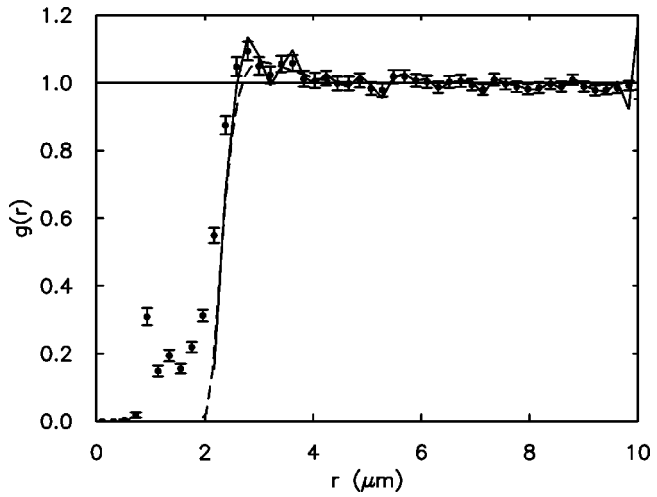

FIG. 2. The projected RDF for the sample of density $\rho=8.0\times10^{-3}$ $\mu\mathrm{m}^{-3}$ (dots), and the result when the unprojection algorithm described in the text is applied (solid line). Also shown is the fit to Eq. (9) (dashed line), as discussed later in the text. The sudden erratic behavior of the unprojected RDF at $r=10$ μm is an artifact of the algorithm which occurs at the upper boundary of the data. The values for the RDF for $r\leqslant1$ μm are unphysical because in that region significant errors arise due to overlapping particles in the images.

effect integrating over the depth of field. Using the projected RDF to extract information about the pairwise potential can lead to incorrect results [8], so understanding how to properly handle projection effects is very important. In Fig. 1, we see two particles within the observation region of depth of field h, defined to be the maximum possible vertical center-to-center distance between two particles which are simultaneously visible under the microscope. The distances between the top of the observation volume and the centers of particles 1 and 2 are denoted by z_1 and z_2, respectively. The distance between the particle centers as seen under the microscope is r, while the actual distance is $\sqrt{r^2+(z_1-z_2)^2}$. Let us define the projected RDF $g_p(r)$ such that the density of particles in the microscope image an apparent distance r away from a particle is given by $ng_p(r)$, where $n=\rho h$ is the projected number density, and ρ is the three-dimensional number density. Thus h can be calculated if ρ is known. Let us assume that the particle distribution is uniform in the z direction, and that the system is isotropic. It can then be shown that the relationship between the three-dimensional RDF $g(r)$ and the projected RDF $g_p(r)$ is given by

$$g_p(r)=\frac{2}{h^2}\int_0^h (h-x)g(\sqrt{r^2+x^2})\,dx. \tag{3}$$

This formula indicates that $g_p(r)$ is simply $g(r)$ smoothed over r values greater than or equal to the projected interparticle distance of interest. This smoothing reduces the RDF's deviations from unity and softens any hard-core-like features. Note that as the depth of field goes to zero, $g_p(r)$ approaches $g(r)$, as it must for an isotropic system [25].

If the density of the system is not too large, then little information is lost due to particles overlapping in the field of view, and an inversion of Eq. (3) is possible using an iterative method. Given a $g_p(r)$, define a sequence $g^{(n)}(r)$ as [26]

$$g^{(0)}(r)=g_p(r), \tag{4}$$

$$g^{(n+1)}(r)=g^{(n)}(r)+g_p(r)-g_p^{(n)}(r), \tag{5}$$

where $g_p^{(n)}(r)$ is the projected version of $g^{(n)}(r)$ obtained from Eq. (3), and we add the condition that if $g^{(n)}(r)<0$ for any r, then we set $g^{(n)}(r)=0$ at that r. We hypothesize that

$$\lim_{n\to\infty} g^{(n)}(r)=g(r). \tag{6}$$

Thus, given an experimentally measured $g_p(r)$, one can determine $g(r)$. Note that in order to calculate $g(r)$ for r larger than some arbitrary r_0, one only needs $g_p(r)$ for $r\geqslant r_0$. Thus, even if the data at small r are unreliable due to statistical and image processing concerns, the unprojection algorithm can still be used to calculate $g(r)$ at large r.

We have not proven analytically that the iteration scheme works, but we have found empirically that it works for hard sphere distribution functions, and converges after 10–100 iterations. Unfortunately, the method is a noise enhancer, that is, any noise in $g_p(r)$ will be enhanced in the calculated $g(r)$. However, even if the statistics in the calculated $g(r)$ are very poor, the method is still useful as a way of estimating the size of the discrepancy between $g_p(r)$ and $g(r)$, and can therefore yield an estimate of the uncertainties due to projection effects in RDF's derived from microscopy data.

Figure 2 shows the RDF from a sample of density 8.0×10^{-3} $\mu\mathrm{m}^{-3}$, and the results after the unprojection algorithm [Eqs. (3)–(6)] is applied to it for $r\geqslant2$ μm. Values of $g_p(r)$ between data points were obtained by linear interpolation, and we set $g_p(r)=1$ for $r\geqslant10$ μm. The depth of field was estimated to be 2.5 μm from the known ρ and n. In this case, the only part of $g(r)$ that is significantly affected by projection is the region where $g(r)$ rises steeply to unity, and even there the correction is small.

Another way to assess projection effects is to vary the effective depth of field h. As h approaches zero, the projected RDF approaches the three dimensional RDF, and thus, by computing the RDF as a function of effective depth of field, one may determine if the finite depth of field is significantly affecting the measured RDF. In order to set an effective depth of field, we must identify characteristics of the par-

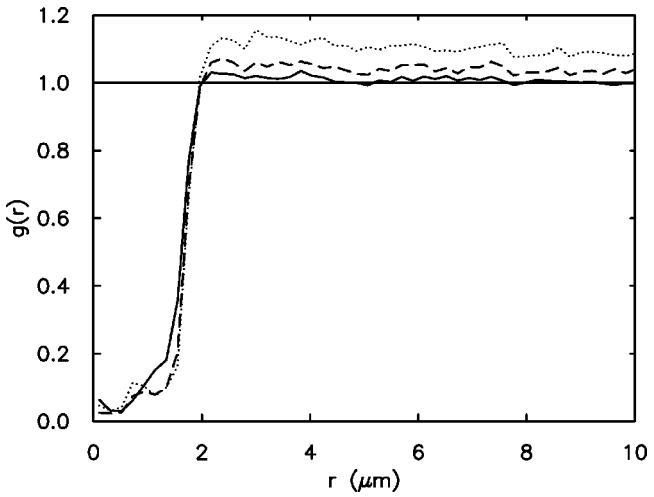

FIG. 3. The RDF for the sample of density $\rho=7.5\times10^{-3}$ μm^{-3}, with the particles thresholded at different brightness levels to achieve effective depths of field (n/ρ) of 1.3 μm (dotted line), 1.7 μm (dashed line), and 2.6 μm (solid line).

ticles that are sensitive to their z position. We found that the particle brightness and radius of gyration are the two parameters that depend most strongly on the distance of the particle from the focal plane. The variation of these parameters with respect to position is approximately symmetric about the focal plane, and therefore one cannot determine the absolute z position of a colloidal particle because of this ambiguity. However, one can use these parameters to set the depth of field by making appropriate cuts.

Figure 3 shows the projected RDF for the sample of density $\rho=7.5\times10^{-3}$ μm^{-3}, for three different effective depths of field. By removing less bright particles from consideration, which were farther from the plane of focus, we changed the effective depth of field, which was calculated using $h=n/\rho$. This technique seemed to work well for $h \gtrsim 2$ μm, but when we tried to select only the brightest particles and hence have the smallest possible depth of field, then the RDF was not properly normalized, i.e., it did not approach unity as r became large. We found that this was because the particles were slightly brighter in one region of the images, so that when the intensity threshold was set too high, only the particles in that small section of the images were selected. However, the calculation of the RDF assumed that the particles were uniformly distributed, which meant that the number density used in the calculation was too small. As seen from Eq. (2), using too small a density causes the calculated RDF to increase from its true value. Thus, making sure that the RDF has the proper normalization is a crucial step in determining whether there is any spatial bias in the data.

Another approach that we found useful in reducing the effective depth of field was to accept only those particles whose radius of gyration was within a certain range. By calibrating against a collection of particles fortuitously adhered to the bottom cover slip in one of our samples, we were able to correlate the radius of gyration (using the Gaussian fitting method) to the distance of the particle from the focal plane. When doing this, it is crucial to first smooth the images by averaging the intensities over a 3×3 neighborhood around each pixel. This reduces the noise in the images, and makes the parameters in the Gaussian fits more reproducible. To set the depth of field, one removes particles whose radius of gyration does not fall within the range dictated by the calibration curve. We used this method on some of our data, and it did not significantly affect our final results. However, the method did provide an independent value of h and hence ρ, which could be compared to the value of ρ calculated from the starting volume fraction and known dilution. The values agreed very well (within 10–30 %), which increased our confidence in the methodology, and indicated that the particles were well dispersed in the samples. Using the radius of gyration instead of the brightness to set the effective depth of field has the advantage of not depending as strongly on the level of fluorescence doping in the particles, which could conceivably vary from particle to particle.

III. RESULTS AND ANALYSIS

We assume that the particles in our samples obey the repulsive part of the DLVO potential given by [13]

$$\frac{U_{\mathrm{DLVO}}(r)}{kT}=Z^2 l_B\left(\frac{e^{\kappa a}}{1+\kappa a}\right)^2\frac{e^{-\kappa r}}{r}, \tag{7}$$

where r is the center to center distance between two spherical colloidal particles with effective charge number Z and radius a, the Bjerrum length $l_B=e^2/(4\pi\epsilon\epsilon_0 kT)\approx0.7$ nm in water (and D_2O) at 23 °C, and

$$\kappa^2=4\pi l_B\sum z_i^2 c_i, \tag{8}$$

where the sum runs over all ionic species of valency z_i and concentration c_i. The Debye screening length $\lambda_D=1/\kappa$ is a measure of the range of the interaction. For pure water, where the only ionic content is due to autodissociation, $\lambda_D=1.0$ μm at 23 °C, while for pure D_2O, $\lambda_D=1.7$ μm at 23 °C [27], so for a mixture of pure H_2O and D_2O, we expect $\lambda_D \gtrsim 1$ μm at 23 °C. In order to have a long-ranged interaction, the ionic content of the suspension must be as low as possible, which was the motivation behind having the ion exchange resin in such close proximity to the colloidal particles. An attractive van der Waals interaction is also present, but at surface-to-surface distances greater than a few nanometers is completely dominated by the repulsive electrostatic component given by Eq. (7), and is thus neglected. The temperature of the samples varied from 21.4 to 24.6 °C, with an average of 23 °C over the course of three days of data collection, which reflects the variation in temperature of the surrounding air, since the samples were not temperature controlled.

The DLVO potential given by Eq. (7) was derived using approximations valid only for low surface potential, or equivalently, small particle charge. However, Alexander *et al.* [28] showed that even when the particles are highly charged, Eq. (7) can still be used with a renormalized charge in place of the ''bare'' charge (the number of ionizable surface groups). This approach has been shown to be valid by observations of the freezing transition in colloids [9,29] as well as by electrophoresis measurements [9]. If the bare charge is used in Eq. (7), then the results are inconsistent with experiment [9]. Similarly, if one assumes that the sur-

face is only partially ionized, and uses the condition of chemical equilibrium of dissociable surface groups to calculate the charge, then that too conflicts with experiment [9]. According to charge renormalization theory, for particles with a large number of ionizable surface groups, the effective charge Z that should be used in Eq. (7) is given by $Z = Ca/l_B$, where a is the radius of the particle, and C is a constant between 4 and 10 [1,2,9]. The exact value of C depends on the number of colloidal particles and ions present, but for the present work, a precise knowledge of Z is not needed, and the above estimate for C will suffice. For the particles used in this work, this gives $Z = 3000–7000$, and we will adopt the intermediate value $Z = 5000$. Since the renormalized charge is smaller than both the bare charge and the charge obtained using chemical equilibrium methods [9], we feel that $Z = 5000$ is a lower limit for the charge that should be used in Eq. (7).

The RDF of a fluid interacting via a strongly repulsive potential $U(r)$ can be well approximated by the expression [30]

$$g(r) \approx y_{\mathrm{HS}}(r/\sigma_{\mathrm{eff}}, \rho\sigma_{\mathrm{eff}}^3) e^{-U(r)/kT}, \tag{9}$$

where $y_{\mathrm{HS}}(r/\sigma_{\mathrm{eff}}, \rho\sigma_{\mathrm{eff}}^3)$ is the RDF of a hard sphere fluid consisting of particles of diameter σ_{eff} and number density ρ, which has been extended to the region $r < \sigma_{\mathrm{eff}}$ in a mathematically consistent way. There is no exact closed form expression for y_{HS}, but since our samples are at such low density, we may approximate y_{HS} by [31]

$$y_{\mathrm{HS}}(r/\sigma_{\mathrm{eff}}, \rho\sigma_{\mathrm{eff}}^3) \approx 1 + \rho\sigma_{\mathrm{eff}}^3 g_1(r/\sigma_{\mathrm{eff}}), \tag{10}$$

where $g_1(r)$ is given by

$$\begin{aligned} g_1(r) &= \pi(r^3/12 - r + 4/3), \quad r \leqslant 2 \\ &= 0, \qquad\qquad\qquad\quad r > 2. \end{aligned} \tag{11}$$

The effective diameter σ_{eff} is given to first order by the expression [32]

$$\sigma_{\mathrm{eff}} = \int_0^\infty (1 - e^{-U(r)/kT}) dr, \tag{12}$$

with higher-order terms adding corrections of less than 1% for $\rho\sigma_{\mathrm{eff}}^3 \lesssim 0.5$ (which is true for all of our samples). For a system of particles in the liquid state interacting via a strongly repulsive potential such as the DLVO potential [Eq. (7)], at $r \approx \sigma_{\mathrm{eff}}$ the RDF begins to depart significantly from zero, making this a useful parameter when describing the range of an interaction.

Figure 4 shows the projected RDF's for four samples of densities 2.4×10^{-4}, 7.3×10^{-4}, 2.5×10^{-3}, and 7.5×10^{-3} $\mu\mathrm{m}^{-3}$, computed using the previously described techniques, with effective depths of field of 2.6, 2.7, 2.6, and 2.7 μm, respectively. Adjusting the depth of field using either intensity or radius of gyration cuts as described in Sec. II D did not significantly affect our final results. These results also did not depend on the distance from the nearest ion exchange resin beads, which was varied from approximately 200 to 3000 μm.

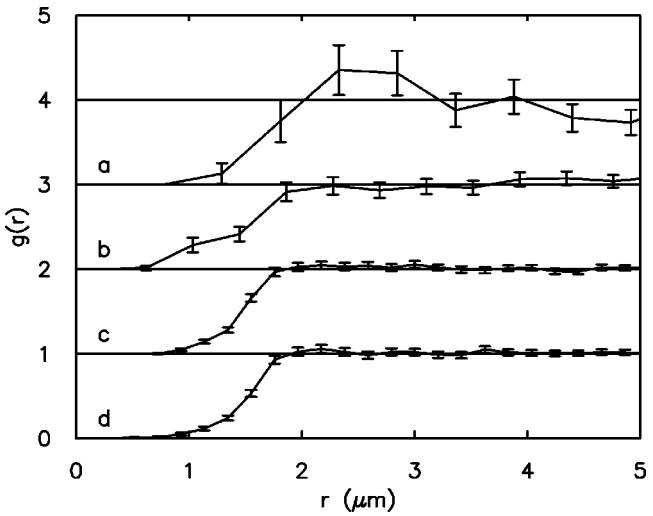

FIG. 4. RDF's for samples of number density (a) 2.4×10^{-4} $\mu\mathrm{m}^{-3}$, (b) 7.3×10^{-4} $\mu\mathrm{m}^{-3}$, (c) 2.5×10^{-3} $\mu\mathrm{m}^{-3}$, and (d) 7.5×10^{-3} $\mu\mathrm{m}^{-3}$. Each graph is offset by successive increments of unity for clarity. The number of images used to create these plots was (a) 3969, (b) 3010, (c) 3050, and (d) 310.

As seen in Fig. 4, all the projected RDF's rise rapidly from zero to unity with no oscillatory structure, and there is no change in the RDF's over a factor of 30 in density, which indicate that the samples are in the dilute limit. We applied the unprojection algorithm of Sec. II D to these RDF's, and then fit the unprojected RDF's to Eq. (9) by eye [evaluated using Eqs. (7) and (10)–(12)], where the steep rise from $g(r) = 0$ to $g(r) = 1$ was considered the most important feature. The RDF's were altered by the unprojection algorithm in a way qualitatively similar to the results in Fig. 2. Since Z was fixed at 5000 ± 2000, this was a single parameter fit for λ_D which yielded Debye lengths of 0.14 ± 0.03, 0.11 ± 0.02, 0.11 ± 0.02, and 0.11 ± 0.02 μm in order of increasing density. The uncertainties in λ_D are mostly due to the uncertainty in Z. If projection effects had not been taken into account, the calculated Debye length would have been 0.02–0.03 μm smaller.

The Debye length is a useful parameter in describing the range of the interaction, but what do we do if the interaction potential is not of the DLVO form as appears to be the case for highly confined colloidal suspensions [3,5,6]? Since $g(r)$ typically rises rapidly from 0 to 1, we might define a phenomenological interaction range by the distance r at which $g(r) = \beta$, where β is between 0 and 1. It is somewhat arbitrary what we choose for β, with $\beta = 1/e$ or $\beta = 0.5$ being ''natural'' choices. However, as is shown in the Appendix, for exponentially decaying potentials (such as DLVO), the effective diameter σ_{eff} given by Eq. (12) can be approximated quite well by $U(\sigma_{\mathrm{eff}})/kT = e^{-\gamma} \approx 0.56$, where $\gamma \approx 0.5772$ is Euler's constant. In the dilute limit, this leads to $g(\sigma_{\mathrm{eff}}) = e^{-e^{-\gamma}} \approx 0.57$. It is very appealing to have our phenomenological interaction range coincide with the effective diameter of Eq. (12) for DLVO-type potentials, so we will choose $\beta = 0.57$, and call the so-defined length scale σ_{eff}. We feel that a length scale defined in this way is a useful phenomenological parameter because it requires no knowledge of the interaction potential, and can be derived directly from the experimental RDF's. This will make it easier to

TABLE I. Projection-corrected effective diameter [using $g(\sigma_{\text{eff}})=0.57$] and Debye length as a function of the age of the sample, which is the time between the construction of the sample cell and the collection of data.

Age (days)	σ_{eff} (μm)	λ_D (μm)	Density (μm^{-3})
5–6	1.9 ± 0.2	0.14 ± 0.03	2.4×10^{-4}
5–6	1.7 ± 0.1	0.11 ± 0.02	7.3×10^{-4}
5–6	1.67 ± 0.03	0.11 ± 0.02	2.5×10^{-3}
9–10	1.70 ± 0.03	0.11 ± 0.02	7.5×10^{-3}
16–17	2.34 ± 0.02	0.20 ± 0.02	8.0×10^{-3}
≈160	1.7 ± 0.3	0.11 ± 0.04	2.5×10^{-3}
≈160	1.8 ± 0.2	0.12 ± 0.03	7.5×10^{-3}

compare the results of different workers' colloidal experiments.

For the data in Fig. 4, the projection-corrected effective diameters [using $g(\sigma_{\text{eff}})=0.57$] are 1.9 ± 0.2, 1.7 ± 0.1, 1.67 ± 0.03, and 1.70 ± 0.03 μm, in order of increasing density. We found that the effective diameters derived from projected RDF's were 0.1–0.2 μm shorter than the projection-corrected effective diameters. For the uncertainties in σ_{eff}, we used the statistical uncertainties in the effective diameters derived from the projected RDF's.

Referring back to Fig. 2, we see the projected RDF for the sample of density 8.0×10^{-3} μm^{-3}, which was constructed approximately one week earlier than the samples whose RDFs are shown in Fig. 4. In the same way as before, the unprojected RDF was fit to Eq. (9) by eye [evaluated using Eqs. (7) and (10)–(12)], and the results are shown in Fig. 2. The projection-corrected Debye length is 0.20 ± 0.02 μm, while the projection-corrected effective diameter [given by $g(\sigma_{\text{eff}})=0.57$] is 2.34 ± 0.02 μm, where the uncertainty was obtained in the same way as described above. Note the small but significant overshoot of unity at $r\approx\sigma_{\text{eff}}$, which is not present in the RDF's of Fig. 4. The height of the peak in the calculated $g(r)$ is consistent with the data. Even at this high density and large effective diameter, however, there is still very little liquid structure, which is characterized by oscillations in $g(r)$, so this system is still close to the dilute limit.

The longer interaction range in this older sample suggests that the ionic strength in this sample was lower than in the other samples, which had Debye lengths of approximately 0.11–0.14 μm. One might conclude that we had not given the ion exchange resin enough time to deionize the samples, because of the apparent decrease in ionic strength over time. To further investigate this, we looked at the sample cells of densities 2.5×10^{-3} and 7.5×10^{-3} μm^{-3}, five months after the initial data were taken [33]. The suspensions appeared the same as they had five months earlier, and very little flocculation had occurred. Unfortunately, the sample of density 8.0×10^{-3} μm^{-3} had evaporated over the five month period, and could thus not be examined. The results for the projection-corrected Debye lengths and effective diameters for these and the earlier samples are summarized in Table I. Since no general trend toward larger interaction ranges was observed over time, we conclude that the samples had in fact been fully deionized at the time of the original data collection.

Before the present research was undertaken, preliminary experiments were performed to determine how extensively water could be purified. Since ionic content is approximately proportional to the conductivity of the solution [34], we used conductivity (or equivalently, resistivity) as our measure of water purity. *p*H is not an adequate purity measure, because, for instance, the addition of NaCl will not affect the *p*H. When water was drawn from a recirculating ion exchange column (Barnstead Nanopure), the column indicated that the resistivity was 18 MΩ cm, which is the resistivity of pure water at 25 °C. However, when we filled a well cleaned plastic bottle with water from the column, transferred a small amount to a glass vial (height, 5 cm, diameter, 2 cm), and then measured the ac conductivity at 200 Hz with an ac bridge [35], the result always lay between 0.7 and 1.5 MΩ cm. The measurement was performed repeatedly with fresh water in order to rinse off any residual ionic impurities on the vial or conductivity probe, and the plateau value is the quoted resistivity.

What can be causing the discrepancy between the column reading of 18 MΩ cm and the measured value of ≈1 MΩ cm? Workers have expressed concern about contamination by atmospheric CO_2 which forms carbonic acid (H_2CO_3) in water [2,3,36]. In fact, when water is in equilibrium with atmospheric CO_2, the resistivity is predicted to be ≈1 MΩ cm (*p*H 5.6) at 23 °C based on Henry's law constant for CO_2 in water and the dissociation constant for carbonic acid [37]. So it might be concluded that atmospheric CO_2 was contaminating the water immediately upon leaving the column, since the resistivity was measured ≈15 min after taking it from the column [38]. To test this idea, we constructed an ion exchange column consisting of a polypropylene tube (diameter, 1.5 cm; height, 12 cm; Bio-Rad No. 732-1010) filled with mixed bed ion exchange resin, and fitted with a stopcock at the bottom to control the flow. This column, along with a sample of water from the Barnstead column, were placed in a glove chamber (I^2R Model X-27-27) which was evacuated and then filled with argon. This evacuation-filling cycle was repeated several times to completely flush the air from the glove chamber. Fresh water was then run through the column repeatedly under the argon atmosphere, and the resistivity reached a plateau at 4.5 MΩ cm. The water was left in the glass vial after the final measurement, and the glove chamber was opened to air. The resistivity subsequently decreased, reaching a final value $\rho_{\text{final}}=0.7$ MΩ cm after approximately 40–50 h. At intermediate times, $1/\rho_{\text{final}}-1/\rho$ decreased approximately exponentially with a characteristic time of 6–8 h. After 30 min, the resistivity was 2.8 MΩ cm, so the absorption of CO_2 into the water appears to be very slow under these conditions (if indeed the drop in resistivity is due to CO_2).

Since we were still unsure as to exactly what ionic impurities were causing the resistivity drop, and the water appeared to be pure while it was in the Barnstead column, we decided to put the ion exchange resin directly into the cell to simulate the chemical environment in the column. We assert that the purity achieved in our sample cells was at least as good as that achieved under the argon atmosphere with our constructed ion exchange column. The resin in the sample cells should have removed any carbonic acid, and we have already shown that absorption of atmospheric CO_2 is a very slow process even under conditions where much surface area

is exposed, so the process should have been even slower in our samples which were well sealed. If the ionic impurities were in fact due to carbonic acid, then a resistivity of $\rho = 5$ MΩ cm would correspond to a Debye length of 0.42 μm at 23 °C ($d\lambda_D/d\rho = 0.04$ μm/MΩ cm). If the ionic impurities were due to NaCl (which typifies lightweight ionic impurities), then a resistivity of 5 MΩ cm would correspond to a Debye length of 0.27 μm at 23 °C ($d\lambda_D/d\rho = 0.03$ μm/MΩ cm) [39]. These results indicate that the Debye lengths in our samples should have been significantly larger than the measured values of 0.11–0.20 μm.

Despite the presence of the ion exchange resin, a significant counterion density due to dissociation from the glass walls and colloidal particles could reduce the Debye screening length below the upper limit of ≈ 1 μm. To simplify the problem, we will do the calculation for pure H_2O. Let us assume that the ion exchange resin removes ions until only H^+ and OH^- remain, and that the equilibrium condition is that for pure water at 23 °C, or $[H^+][OH^-] = 0.9 \times 10^{-14}$ mol^2 L^{-2} [27]. If the particle number density is 8.0×10^{-3} μm^{-3}, then, after imposing charge neutrality, and taking into account the geometry of our sample cell, we obtain that the Debye length is approximately 0.8 μm if the charge density on the glass surfaces is $0.05e$/nm^2 and 0.9 μm if the charge density is $0.005e$/nm^2. The latter charge density is the value Kayser quoted when he analyzed the wetting of a glass surface by water [40]. These calculated Debye lengths will increase if the D_2O in the sample cells is taken into account, or if a smaller particle number density is used. Therefore, the contribution of counterions from the glass surfaces and the particles also cannot explain the short Debye lengths.

IV. DISCUSSION

A. Could the presence of the glass wall have an effect on the results?

Some recent papers by Muramoto *et al.* and Ito *et al.* [10] raised the concern that the bottom glass cover slip may have influenced the structure of the suspension, even if the cover slip was 100–1000 Debye lengths from the region where we took data. In their work, they studied the distribution of colloidal particles near a naturally charged glass plate. They found that approximately 5 μm from the glass plate, the particle density was about a factor of 2 or 3 higher than in the bulk, and the density decreased very slowly with distance from the plate, assuming the bulk value around 50 μm from the plate. What is very unexpected about this result is that they see the same phenomenon regardless of the density of the suspending medium (ranging from 1.00 to 1.06 g/cm^3), and it persists even in the presence of high levels of added salt, up to NaCl concentrations of about 10^{-4} mol/L. This NaCl concentration would correspond to a Debye length of 0.03 μm, which should completely screen out interactions on length scales greater than about 0.3 μm. That significant structure was seen out to 50 μm suggests that some ultra-long-ranged interaction is present.

In order to see if this effect was present in our sample cells, we made a cell according to the same protocol described in Sec. II A, except the suspending medium was a solution of deionized H_2O and KCl of concentration 4×10^{-5} mol/L, corresponding to a concentration of NaCl for which Muramoto *et al.* and Ito *et al.* saw their condensation effect. No ion exchange resin was present in the sample cell. Figure 5 shows the number of particles $N(z)$ as a function of distance from the bottom cover slip, which was obtained by averaging together the results of 25 independent scans through the sample. Note that $N(z)$ is actually the number of particles in the region between $z - h/2$ and $z + h/2$, where h is the depth of field. If the number density of particles decays exponentially with distance from the bottom cover slip, then $N(z)$ will decay exponentially as well, with the same characteristic length scale. At $z = 0$, half of the field of view is below the glass plate, where there are no particles, so $N(z)$ initially increases with z as more of the field of view enters the sample volume. Thus $N(z)$ should reach a maximum at $z \approx h/2$, where h is the depth of field, and then decay exponentially with a scale height given by $3kT/(4\pi a^3 \Delta\rho g)$, where $\Delta\rho$ is the difference in density between the particles and the suspending medium. The number of particles reached a maximum at 5 μm instead of $h/2 \approx 1.5$ μm, which could be due to electrostatic repulsion from the wall. The solid line in Fig. 5 shows the best fit to an exponential for the region $z \geq 7$ μm, which gives a scale height of 17.5 ± 0.1 μm, corresponding to a particle density of 1.049 ± 0.002 g/cm^3. This is in good agreement with the value of 1.05 g/cm^3 quoted by Polysciences. Since we saw the expected exponential decay in particle density, with no evidence of ultra-long-range structure, we conclude that the phenomenon occurring in Muramoto *et al.* and Ito *et al.*'s work was not present in our samples, and we assert that the glass cover slip did not affect the bulk structure.

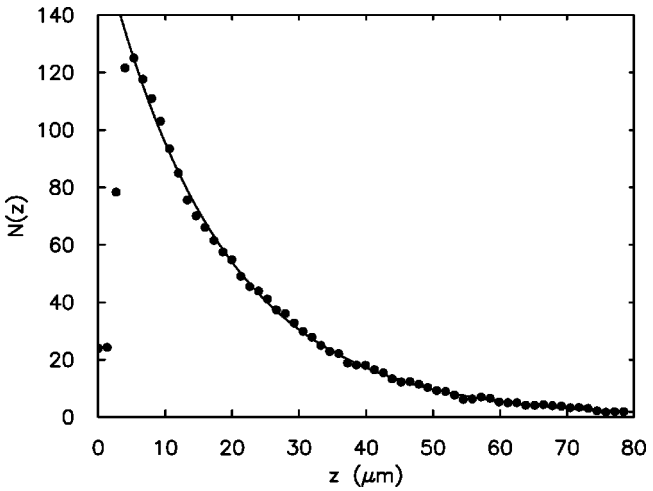

FIG. 5. The number of particles $N(z)$ observed at a distance z from the bottom cover slip (dots), and the best-fit exponential $N(z) = 169\ e^{-z/17.5\ \mu m}$ (line) for $z \geq 7$ μm.

B. Comparison of results to the literature

Our results are surprising, as given our careful sample preparation and the direct presence of the ion exchange resin, we expected to have an ionic strength approaching that of a chemically pure environment, which would have led to an interaction range much larger than we observed. In fact, for particles of diameter 1 μm suspended in pure H_2O, $\sigma_{\text{eff}} \approx 8$ μm ($\lambda_D = 1.0$ μm), while for pure D_2O, $\sigma_{\text{eff}} \approx 13$ μm

TABLE II. A summary of interaction measurements in aqueous colloidal suspensions of low ionicity. It includes bulk visualization experiments where microscopy was used to directly image the particles in the bulk, confined visualization experiments in which the particles were directly imaged in a confined geometry, and scattering experiments. In bulk experiments and confined experiments, the number density is given in units of μm^{-3} and μm^{-2}, respectively. A question mark in the table indicates that the information could not be obtained from the reference. Since the confined experiments gave results that could not be explained with DLVO theory, such as attractive interactions, no attempts were made to extract the DLVO parameters Z and λ_D, and hence that part of the table is left blank. The effective diameter was calculated, when possible, using the approximation $g(\sigma_{eff})=0.57$, or in some cases, using $U(\sigma_{eff})/kT=0.56$.

	Directly measured parameters			DLVO parameters		
Experiment type	Diameter (μm)	Number density[a] (μm^{-3} or μm^{-2})	σ_{eff} (μm)	λ_D (μm)	$Z l_B/a$	Ref.
Bulk visualization[b]	0.979	$(0.24–8.0)\times10^{-3}$	1.7–2.3	0.11–0.20	7	Present work
(low density)	0.652	0	2.9	0.272	13[c]	[3]
	0.97	0	3.4	0.268	20[c]	[3]
	0.97	0	?	0.100 ± 0.010	?	[3]
	1.53	0	4.2	0.289	21[c]	[3]
	0.65	0	1.6	0.161 ± 0.010	4	[2]
	0.996	0	3.3	0.320 ± 0.030	7	[1]
	0.770	?	1.6	0.42[d]	0.35[d]	[4]
Confined visualization[e]	1.27	$(5.8–24)\times10^{-3}$	1.4–3.5			[5]
(low density)	0.5	0.092–0.26	0.5–0.6			[6]
	0.97	0	1.5–1.8			[3]
	1.53	0	2.4			[3]
Bulk scattering[f]	0.080	1.8		0.38[g]	9	[11]
(high density)	0.091	3.4		$\gtrsim0.15$	?	[7]

[a]A zero in this column indicates that although a value for the number density is not given in the reference, we believe that the researchers were working at effectively infinite dilution.

[b]In Refs. [1–3], pairs of particles were positioned close to each other using optical tweezers, and then released. By tracking the particles' motion, these workers were able to solve the master equation for the equilibrium RDF. The RDF was then inverted to yield the interaction potential, which was then fit to DLVO theory [Eq. (7)] with Z and λ_D as adjustable parameters. In Ref. [4], the RDF was computed using digital microscopy methods similar to those in the present work, and the resulting interaction potential was fit to DLVO theory in the same way as described above.

[c]After fitting the interaction potential to DLVO theory [Eq. (7)], the resulting particle charges were 2–3 times larger than would be expected by charge renormalization theory. If one fixes Z to be more in line with charge renormalization theory ($Z l_B/a\approx7$), and allows only λ_D to vary, then the resulting values for λ_D for these entries would be 0.32–0.38 μm, but the fit is poor.

[d]In Ref. [4], a small amount of NaCl (0.5×10^{-6} mol/L) was added to one of the suspensions. The measured Debye length is in agreement with the expected Debye length calculated from the NaCl concentration. In fact, their Debye length is greater than all other results in the table, for which the workers attempted to deionize their samples *in situ*. However, their best fit value for Z is much lower than charge renormalization theory predicts. If one sets $Z l_B/a=7$, and allows λ_D to vary, then one obtains $\lambda_D\approx0.13$ μm, but the resulting potential fits the data very poorly. We suspect that their data suffers from projection effects, so unprojecting their data would cause a steepening of the RDF at $r\approx\sigma_{eff}$, which would lead to higher Z and lower λ_D.

[e]In Ref. [3], the experiment was performed as described in footnote b. In Refs. [5,6], the RDF was obtained using digital microscopy methods similar to those in the present work.

[f]In Ref. [11], the structure factor $S(q)$ of the suspension was determined via light scattering, which was fit to DLVO theory [Eq. (7)] using charge renormalization theory and the rescaled mean spherical approximation using no adjustable parameters. In Ref. [7], the suspension had solidified, and we calculated a lower limit to the Debye length using charge renormalization theory and a phase diagram for colloidal systems [41].

[g]Even though the suspension in Ref. [11] was strongly deionized, the high number density of particles led to a large counterion density, which reduced the maximum screening length significantly below that of pure water. The value for λ_D given here is in good agreement with the maximum screening length calculated using the counterion density.

($\lambda_D=1.7$ μm). Even if we relax our standards for purity to that of water with resistivity 5 MΩ cm, which can be achieved in the bulk (see Sec. III), we should have had $\sigma_{eff}\gtrsim3$ μm ($\lambda_D\gtrsim0.27$ μm). In recent years, there have been many experiments on interactions in colloidal systems using direct visualization methods [1–6] as in the present work, and also using scattering techniques [7,11]. In order to put our results in context, in Table II we summarize the results of experiments performed under similar conditions, i.e., aqueous medium, charged polymer spheres, and low ionicity. All of the systems shown in the table are at very low number density except for those used in the scattering experiments.

The bulk visualization experiments [1–4] are most like the present work. These experiments were done far from

confining walls, and with the exception of Ref. [4], these workers attempted to deionize *in situ* by placing ion exchange resin in the sample cell, but not in close proximity ($\gtrsim 5$ mm) to the region where data were taken. These experiments yielded Debye lengths ranging from 0.10 to 0.42 μm. However, the Debye length of 0.42 μm obtained in Ref. [4] is hard to understand, as explained in footnote d in Table II. Our results for the Debye length fall in the low end of this range. Our effective diameters also fall well below the values of 3.3 and 3.4 μm reported for suspensions in which the particles had a diameter approximately equal to that in the present work, ≈ 1 μm. This is surprising, since we regard our sample preparation to be at least as good if not better than that of other workers.

The results on confined suspensions [3,5,6] are less relevant to the present work, but are still of some interest. These experiments showed that when the height of the sample cell is less than a few particle diameters, the particles experience an attractive interaction not accounted for in DLVO theory. The depth of the attractive well is of the order of $(0.1–1)kT$, and occurs much too far away from the particle to be due to a van der Waals interaction. If we ignore the attractive well, and calculate an effective diameter using $g(\sigma_{\text{eff}})=0.57$, then Table II shows that the interaction range (σ_{eff}) varies significantly among the experiments. Using the concept of an effective diameter instead of the Debye length to describe the interaction range is especially important in this case because the DLVO potential does not seem to apply to highly confined suspensions. These workers had ion exchange resin in their samples, but due to geometrical constraints, the ion exchange resin was far away ($\gtrsim 5$ mm) from the region of data collection. The range of the interaction in confined systems appears to be somewhat smaller than in the bulk, perhaps due to the larger role that counterions play in a smaller sample volume.

Finally, for completeness, the results of two representative scattering experiments [7,11] are also present in Table II. In order to obtain a strong scattering signal that is not complicated by the individual particle structure, scattering experiments typically involve very dense suspensions of small particles ($a \lesssim 50$ nm). Since one is in the high density regime, it is difficult to obtain information about the pairwise interactions. In addition, the large number of particles leads to a significant counterion density, which reduces the maximum Debye length from its value in pure water of ≈ 1 μm. Therefore, obtaining a Debye length significantly smaller than 1 μm in such experiments would not be at all surprising. In fact, the value shown in the table for λ_D from Ref. [11] is in good agreement with the maximum possible screening length calculated from the counterion density.

C. Colloidal particle screening

Netz and Orland recently presented a new theory of colloidal interactions using field theory techniques, which goes beyond DLVO theory by including non-mean-field effects such as fluctuations and multibody correlations [12]. For large particle separations, their expression for the interparticle potential has the form $U(r)\sim e^{-\kappa_{\text{NO}}r}/r$, where κ_{NO} is given by Eq. (8), except that the sum now includes the colloidal particles in addition to the ions, i.e., $\kappa_{\text{NO}}^2=4\pi l_B Z^2\rho + \kappa^2$. Thus, their theory predicts that the colloidal particles themselves contribute to the electrostatic screening, and not just the ions. This is an intriguing concept, as such an effect could explain our observed short-ranged interaction. Unfortunately, quantitative comparison with their theory is impossible, as they wrote $U(r)$ as a series expansion containing first and second order terms, and the second order term is 4–5 orders of magnitude larger than the first order term for our experimental conditions (and for all other workers' experiments performed thus far at finite dilution). This strongly suggests that experiments up to now at finite dilution are outside the range of applicability of their series solution [42]. It would be interesting to see if including a third order term could make a comparison with our experiment possible.

V. CONCLUSIONS

We have presented experimental protocols and data analysis techniques that were designed to overcome two difficulties affecting workers who use direct visualization methods in colloidal studies: how to maintain a very low ionicity in the surrounding medium, and how to systematically handle projection effects. We applied these techniques to a series of colloidal suspensions of polystyrene microspheres in a H_2O/D_2O mixture. We found that the interactions between the particles were surprisingly short ranged, with projection-corrected effective diameters of 1.7–2.3 μm ($\lambda_D = 0.11–0.20$ μm). This interaction range is very short compared to the theoretical upper limit of $\sigma_{\text{eff}}\approx 8$ μm ($\lambda_D\approx 1$ μm) for micron sized particles, and compared to the value $\sigma_{\text{eff}}\gtrsim 3$ μm ($\lambda_D\gtrsim 0.27$ μm) in water of resistivity 5 MΩ cm, which we could prepare in the bulk, and felt that we could attain in our sample cells. If we had not corrected for projection effects, σ_{eff} and λ_D would have been smaller by 0.1–0.2 and 0.02–0.03 μm, respectively.

We are satisfied with our sample preparation and our handling of projection effects, but are puzzled by our results. Our experiment is unique among the literature cited in Table II, in that we had ion exchange resin in the sample cell in direct contact with the suspension, which we felt should have led to screening lengths at least as long as those obtained by other workers who did not have ion exchange resin in such close proximity to the data collection region. Our measured screening lengths were also far shorter than what we feel we have achieved using bulk purification methods (see Sec. III), and we believe that the presence of ion exchange resin directly in the sample cell should have yielded better results than the bulk cleaning methods. Furthermore, our results were the same regardless of the distance from the ion exchange resin, and no collective motion of the colloidal particles was observed, which argues against large ion gradients in the sample.

Other researchers have also fallen far short of the maximum possible Debye length in spite of extensive cleaning procedures (see Table II). This, coupled with the large variation in the Debye lengths between different experiments, suggests that work needs to be done in finding the source of the impurities in the surrounding medium that is causing the greater than expected screening. Arguments that airborne CO_2 is a significant source of ions are not compelling, as discussed in Sec. III. Before these questions are answered,

efforts to understand even more complicated phenomena such as confinement induced attractions will be hampered.

The difficulties in preparing ultrapure water (see Sec. III), as well as the concern expressed above, lead us to believe that water is not the best suspending medium for experiments requiring long screening lengths. Perhaps a better medium can be found that is nondissociable (unlike water), in order to minimize the ionic concentration. This medium would also have to be polar so that the surface groups on the particles would dissociate. Such a system might have fewer experimental complications than an aqueous system.

ACKNOWLEDGMENTS

We would like to thank David Weitz for generously allowing us to use his confocal microscope at the University of Pennsylvania, and Eric Weeks for his extensive assistance with the operation of the microscope. We also appreciate their helpful comments as well as those of John Crocker, Frank Hicks, Neil Ashcroft, Don Koch, David Grier, Seth Fraden, Cherry Murray, Jane Cerise, Thomas Palberg, Hector Abruna, and Geoffrey Chester. We are also grateful to Carol Bayles and Watt Webb for their assistance. R. D. wishes to acknowledge support from the National Science Foundation. Financial support was provided by the National Science Foundation through Grant No. DMR-9320910, and we also made use of the Cornell Center for Materials Research facilities supported by the NSF under Grant No. DMR-9632275.

APPENDIX

Here we will show that the effective diameter $\sigma_{\rm eff}$ given by Eq. (12) can be approximated by $U(\sigma_{\rm eff})/kT=e^{-\gamma}$, where $\gamma\approx0.5772$ is Euler's constant. Setting $\Phi(r)=U(r)/kT$, and integrating Eq. (12) by parts, we obtain

$$\sigma_{\rm eff}=-\int_0^\infty r\Phi'(r)e^{-\Phi(r)}dr. \tag{A1}$$

Changing the integration variable to $u=\Phi(r)$, and asserting that $\Phi(0)\approx\infty$, we obtain

$$\sigma_{\rm eff}=\int_0^\infty \Phi^{-1}(u)e^{-u}du. \tag{A2}$$

For DLVO-type potentials of the form $\Phi(r)\sim e^{-\kappa r}/r$, the exponential factor dominates the behavior, so we will set $\Phi(r)=Ae^{-\kappa r}$. Putting this into Eq. (A2), we obtain

$$\sigma_{\rm eff}=(\ln A)/\kappa+\gamma/\kappa, \tag{A3}$$

where we have used $\int_0^\infty e^{-x}\ln x\,dx=-\gamma$. After some rearranging, Eq. (A3) becomes $\Phi(\sigma_{\rm eff})=Ae^{-\kappa\sigma_{\rm eff}}=e^{-\gamma}$, which is what we set out to prove.

This approximation is essentially exact for a potential of the form $U(r)\sim e^{-\kappa r}$ if the prefactor is large. For DLVO potentials with $Z=5000$ and $a=0.5$ μm, the error in $\sigma_{\rm eff}$ increases from 0.004% to 0.1% as λ_D is varied from 0.05 to 1 μm. The error decreases with increasing Z and decreasing λ_D. By comparison, with the first order approximation $U(\sigma_{\rm eff})/kT\approx1$ [43], the error increases from 2% to 6% when λ_D is varied over the same range.

[1] J. C. Crocker and D. G. Grier, J. Colloid Interface Sci. **179**, 298 (1996).
[2] J. C. Crocker and D. G. Grier, Phys. Rev. Lett. **73**, 352 (1994).
[3] J. C. Crocker and D. G. Grier, Phys. Rev. Lett. **77**, 1897 (1996).
[4] K. Vondermassen, J. Bongers, A. Mueller, and H. Versmold, Langmuir **10**, 1351 (1994).
[5] G. M. Kepler and S. Fraden, Phys. Rev. Lett. **73**, 356 (1994).
[6] M. D. Carbajal-Tinoco, F. Castro-Román, and J. L. Arauz-Lara, Phys. Rev. E **53**, 3745 (1996).
[7] T. Palberg, W. Härtl, U. Wittig, H. Versmold, M. Würth, and E. Simnacher, J. Phys. Chem. **96**, 8180 (1992).
[8] K. S. Rao and R. Rajagopalan, Phys. Rev. E **57**, 3227 (1998).
[9] T. Palberg, W. Mönch, F. Bitzer, R. Piazza, and T. Bellini, Phys. Rev. Lett. **74**, 4555 (1995).
[10] T. Muramoto, K. Ito, and H. Kitano, J. Am. Chem. Soc. **119**, 3592 (1997); K. Ito, T. Muramoto, and H. Kitano, *ibid.* **117**, 5005 (1995).
[11] W. Härtl, H. Versmold, and U. Wittig, Langmuir **8**, 2885 (1992).
[12] R. R. Netz and H. Orland, Europhys. Lett. **45**, 726 (1999).
[13] E. J. W. Verwey and J. Th. G. Overbeek, *Theory of the Stability of Lyophobic Colloids* (Elsevier, New York, 1948).
[14] Polysciences technical support.
[15] The glass parts used in constructing the sample cell were cleaned by sonication at 50–60 °C for 15–30 min in a solution of Pex (Peck's Products Co.) and distilled water (three times in fresh solutions), followed by distilled water (three times), acetone (one time), methanol (three times), distilled water (three times), and finally deionized water (two times).
[16] We inserted partial Teflon rings into some of the cells, but this provided no experimental advantage.
[17] John Crocker (personal communication).
[18] In previous work where we used a phase contrast microscope [R. V. Durand and C. Franck, Phys. Rev. E **56**, 1998 (1997)], the depth of field was approximately 10 μm, compared to 2–3 μm for the present work.
[19] Leica DMIRB with a Noran Instruments OZ confocal attachment.
[20] The background intensity at a given point was estimated by averaging the intensities of the pixels within a circle of radius equal to the CG background subtraction length scale. This local background intensity was subtracted from the original image.
[21] If a given pixel has the brightest intensity in a circular region around that pixel, then the pixel is called a candidate particle. By looking in more detail at the intensity profile around each candidate particle, spurious particle identifications can be

eliminated. The CG candidate particle length scale is the radius of the circular region used to determine the candidate particles.

[22] The intensity weighted zeroth, first, and second position moments were calculated for the intensity profile of each particle using a circular region. The radius of this region is the CG moment calculation length scale.

[23] The brightness (zeroth moment) is the sum of pixel intensities of the particle over a circular region equal to the CG moment calculation length scale.

[24] When using the moment calculation method, the radius of gyration is defined to be $\sqrt{\langle x^2\rangle_I+\langle y^2\rangle_I}$, where $\langle\ \rangle_I$ indicates the intensity weighted average in the coordinate system defined by the principal axes of the particle. When using a Gaussian fit, the radius of gyration is defined to be $\sqrt{\sigma_x^2+\sigma_y^2}$, where σ_x and σ_y are the characteristic lengths of the Gaussian profile in the x and y directions, respectively [see Eq. (1)].

[25] Ironically, however, having $h=0$ would be too much of a good thing, because in that case, no particles would be seen, and thus no RDF could be computed. So a finite depth of field is always needed in colloidal microscopy.

[26] Equation (5) is a specific case of the more general iteration scheme $g^{(n+1)}(r)=g^{(n)}(r)+\alpha[g_p(r)-g_p^{(n)}(r)]$. We have found that $\alpha=1$ works fine for our purposes, but it is possible that smaller values could lead to better convergence properties in other cases.

[27] Ionization constants for H_2O and D_2O were obtained from *CRC Handbook of Chemistry and Physics*, 80th ed., edited by D. R. Lide (CRC Press, New York, 1999), p. 8-85.

[28] S. Alexander, P. M. Chaikin, P. Grant, G. J. Morales, and P. Pincus, J. Chem. Phys. **80**, 5776 (1984).

[29] Y. Monovoukas and A. P. Gast, J. Colloid Interface Sci. **128**, 533 (1989).

[30] J. D. Weeks, D. Chandler, and H. C. Andersen, J. Chem. Phys. **54**, 5237 (1971).

[31] F. H. Ree, R. N. Keeler, and S. L. McCarthy, J. Chem. Phys. **44**, 3407 (1966).

[32] L. Verlet and J.-J. Weis, Phys. Rev. A **5**, 939 (1972). Since $U(r)=\infty$ for $r<2a$, we should write $\sigma_{\rm eff}=2a+\int_{2a}^{\infty}(1-e^{-U(r)/kT})dr$, where $U(r)$ is given by Eq. (7). However, since $U(2a)\gg kT$, Eq. (12) is essentially exact without explicitly including the hard-sphere repulsion.

[33] The microscope used for the original data collection was not readily available at this later time, so instead, we used a Zeiss Axiovert 10 inverted microscope equipped with a Bio-Rad MRC600 confocal attachment.

[34] S. H. Maron and C. F. Prutton, *Principles of Physical Chemistry*, 4th ed. (Macmillan, New York, 1968), Chap. 11.

[35] We used an immersion conductivity probe with platinum electrodes (Yellow Springs Instrument Company, No. 3403).

[36] T. Palberg and M. Würth, Phys. Rev. Lett. **72**, 786 (1994).

[37] Henry's law and dissociation constants were obtained from H. S. Harned and R. Davis, J. Am. Chem. Soc. **65**, 2030 (1943). In using their results, we have set the activity coefficients for H^+ and HCO_3^- equal to unity, which is a valid assumption due to the very low concentrations of these ions.

[38] One possible reason for the discrepancy between the resistivity reading given by the Barnstead column and the value measured outside the column is that inside the column, the water could be in a nonequilibrium state where the carbonic acid (H_2CO_3) has not dissociated, and thus the water appears pure. When the water is taken out of the column, and is away from the ion exchange resin, the carbonic acid dissociates, donating ions which subsequently lower the resistivity.

[39] The necessary data to relate resistivity to ionic concentration and hence Debye length are given in S. H. Maron and C. F. Prutton, *Principles of Physical Chemistry*, 4th ed. (Ref. [34]), Chap. 11.

[40] R. F. Kayser, Phys. Rev. Lett. **56**, 1831 (1986).

[41] M. O. Robbins, K. Kremer, and G. S. Grest, J. Chem. Phys. **88**, 3286 (1988).

[42] An interesting numerical coincidence occurs with our data of density $\rho\geqslant 2.5\times 10^{-3}\ \mu\mathrm{m}^{-3}$. The screening lengths predicted for our systems by Netz-Orland theory are much shorter than those predicted by DLVO theory, but the factor multiplying the exponential is large enough to yield reasonable values for the effective diameter. The Netz-Orland theory was formulated for point particles, but if their potential $U(r)$ is multiplied by the DLVO-like finite size correction factor $e^{2a\kappa_{\rm NO}}/(1+a\kappa_{\rm NO})^2$, then the effective diameter predicted by Netz-Orland for our systems is 1.4–1.7 μm, in quantitative agreement with most of our experimental data. However, this agreement is surely fortuitous, as the theory predicts a very strong dependence of $\sigma_{\rm eff}$ on ρ, which we did not observe.

[43] W. B. Russel, D. A. Saville, and W. R. Schowalter, *Colloidal Dispersions* (Cambridge University Press, Cambridge, 1991), p. 345.